

0.8–2.5 MICRON SPECTROSCOPY OF NOVA OPHIUCHI 1998¹

DAVID K. LYNCH, RICHARD J. RUDY, AND S. MAZUK

The Aerospace Corporation, P.O. Box 92957, Los Angeles, CA 90009; david.k.lynch@aero.org, richard.j.rudy@aero.org, stephan.m.mazuk@aero.org

AND

RICHARD C. PUETTER

Center for Astrophysics and Space Science, University of California at San Diego, La Jolla, CA 92093-0424

Received 1999 September 10; accepted 2000 April 14

ABSTRACT

We report 0.8–2.5 μm spectroscopy of the very fast Nova Ophiuchi 1998 from June 19 and 22 to October 2.15 1998 UT. On the first night the Paschen and Brackett emission lines dominated the spectrum, although He I 1.0830 μm was the strongest single line present and He II was very weak. There were also broad, symmetric emission wings underlying the H I and He I lines with FWHM of about 10,000 km s^{-1} . Three nights later the rapid evolution of the nova to higher excitation conditions was evident from the much stronger He II lines which had increased by a factor of 4 relative to the hydrogen lines. The C III line at 0.9710 μm also appeared the second night, a line that we have heretofore seen only in Wolf-Rayet stars and which almost certainly indicates an overabundance of carbon. The broad emission wings were also present. About 110 days later on October 2.15 UT, the emission lines were very weak (5%–15% of the continuum) and only a few Paschen features and lines of He II were present. At no time during our observations was there any evidence of a long-wavelength upturn indicative of thermal emission from dust. The continuum magnitudes on the dates of observation at J (1.25 microns) were 9.4, 10.9 to 15.0, respectively. The optical decline of 0.37 mag day^{-1} makes this nova one of the fastest ever seen. Model fits of the broad lines profiles suggest that they originate in an optically thin, spherically expanding shell. The line ratios from the narrow components deviate significantly from case B values and seem to come from an optically thick ($\tau = 10$ –100 at line center in Pa α), high-density ($n_e \sim 10^{11} \text{ cm}^{-3}$) gas at around 10,000 K.

Subject headings: infrared: stars — novae, cataclysmic variables — radiative transfer — stars: winds, outflows

1. INTRODUCTION

Novae are one of three types of objects that significantly enrich the interstellar medium with heavy elements (supernovae and stellar winds from giant stars being the others). A nova begins as a close binary system in which a late-type main-sequence star fills its Roche lobe and transfers material to an accretion disk where it ultimately reaches the surface of the white dwarf. A thermonuclear runaway (TNR) in the white dwarf's predominantly hydrogen envelope takes place when enough matter accumulates on the surface of the white dwarf to ignite. TNR in fast novae probably requires that the abundance of CNO nuclei be enriched in the envelope of the white dwarf, while slow novae may have more normal CNO abundances in the shell-burning region. Theoretical models support the idea that nova speed is correlated with CNO abundances in the shell-burning region (see Starrfield 1989 for a review). These models also predict that CNO abundances in the nova ejecta will be enhanced above cosmic values in amounts correlated with the abundance of CNO in the shell-burning region and with the speed of the nova. There is, in fact, some empirical evidence for this correlation between nova speed and CNO abundances in the nova ejecta (Williams et al. 1978; Williams & Gallagher 1979; Gallagher et al. 1980).

Enhancement of CNO abundances in the shell-burning region could occur in the course of the mass transfer onto

the WD; however, this would require an enormous amount of CNO in the companion star's atmosphere. A more likely possibility is that the accreted material contains nearly cosmic abundances but somehow becomes mixed with carbon and oxygen from the white dwarf (MacDonald 1984; Prialnik & Kovetz 1984), at least for a CO white dwarf. In either event, once the accreted envelope burns, the energy release heats the envelope and ejects some fraction of it, enriching the interstellar medium. In view of this possible relationship between CNO abundances in nova ejecta and the thermonuclear processes occurring in the nova shell burning region, observations that provide insight into the abundances of CNO in nova ejecta provide important observational constraints on theoretical models. Observations of Nova Ophiuchi 1998 are valuable in this regard because it was a very fast nova and its near-IR spectrum showed evidence of CNO excesses.

Nova Ophiuchi 1998 was discovered photographically by Nakano et al. (1998) on 1998 June 15.561 UT. No object brighter than 15th magnitude was present at this position as late as 1998 May 19. Its position given by Hanzl (1998) is $\alpha = 17^{\text{h}}31^{\text{m}}59^{\text{s}}.79$, $\delta = -19^{\circ}13'56''$ (2000), corresponding to Galactic coordinates $l = 6^{\circ}$, $b = 7^{\circ}.8$. The precise date of outburst is unknown but is believed to be a few days prior to discovery based on optical spectroscopy and the nova's monotonically decreasing brightness. On June 18 the object showed strong emission lines of H I and He I superposed on a featureless continuum (Filippenko et al. 1998). H α had a base width of 12,000 km s^{-1} and a core width of 2000 km s^{-1} . Kato reports that the position of the nova is within the

¹ This work supported by the Aerospace Independent Research and Development Program.

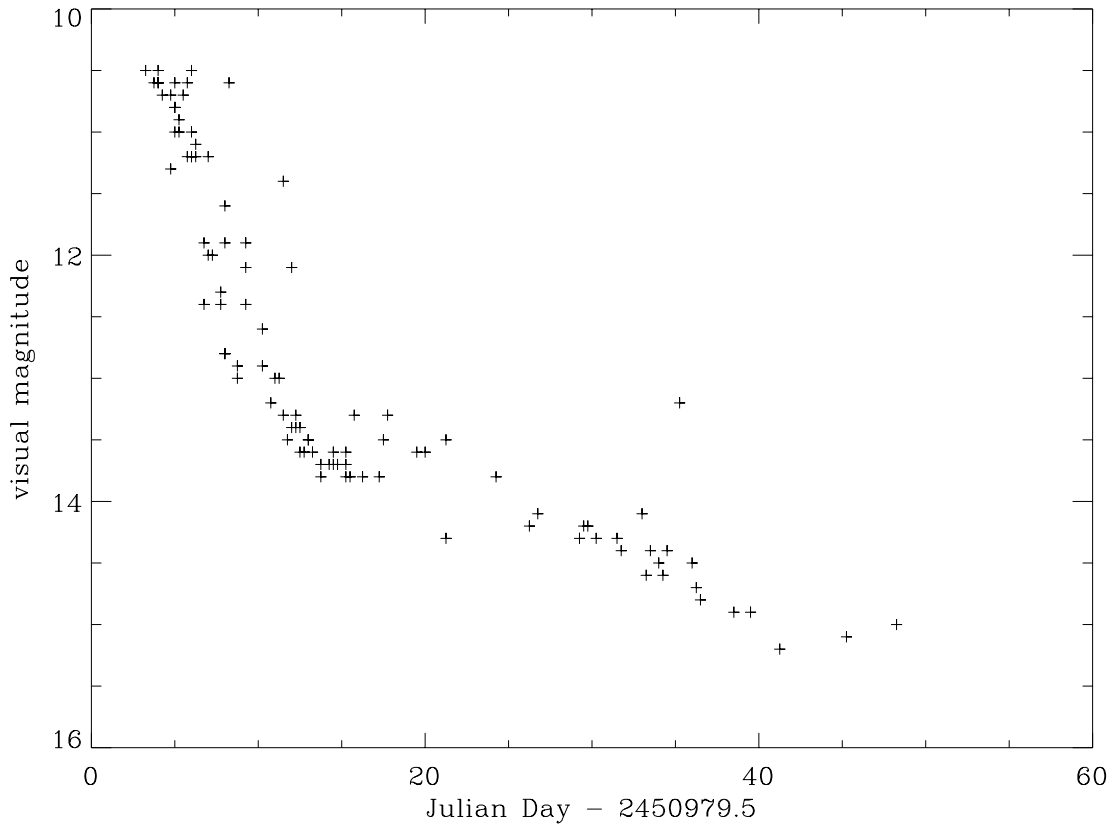


FIG. 1.—Light curve of Nova Ophiuchi 1998. Note the rapid decline during the first 18 days after outburst ($0.32 \text{ mag day}^{-1}$), followed by a slower decline between day 18 and day 45 ($0.05 \text{ mag day}^{-1}$). After about 45 days the decline halted, and the nova remained near $m_v = 15$. There was no evidence of dust formation. (Light curve courtesy J. Mattei at the AAVSO.)

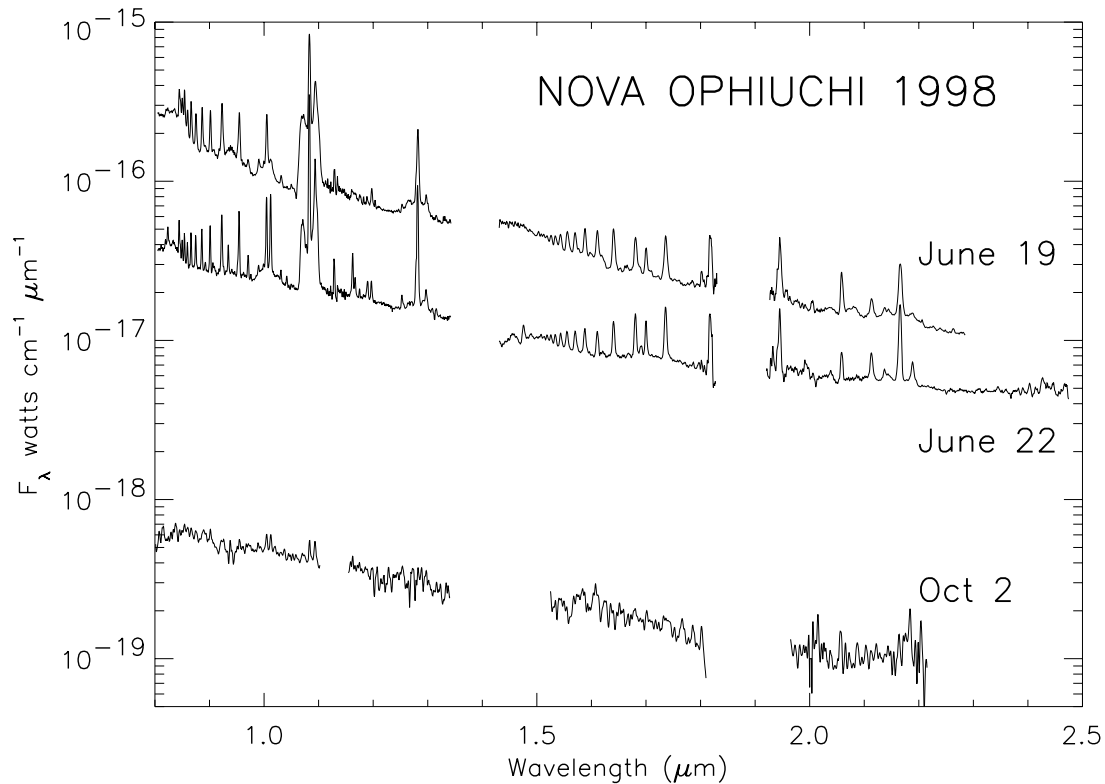


FIG. 2.—Three spectra of Nova Ophiuchi 1998 taken on 1998 June 19.40, June 22.37, and October 2.15, all UT. Note the pedestals under the H I Pa δ , Pa β , and He I $\lambda 1.0830$ lines. Also note the difference in the Paschen and Brackett lines between the 19th and 22nd.

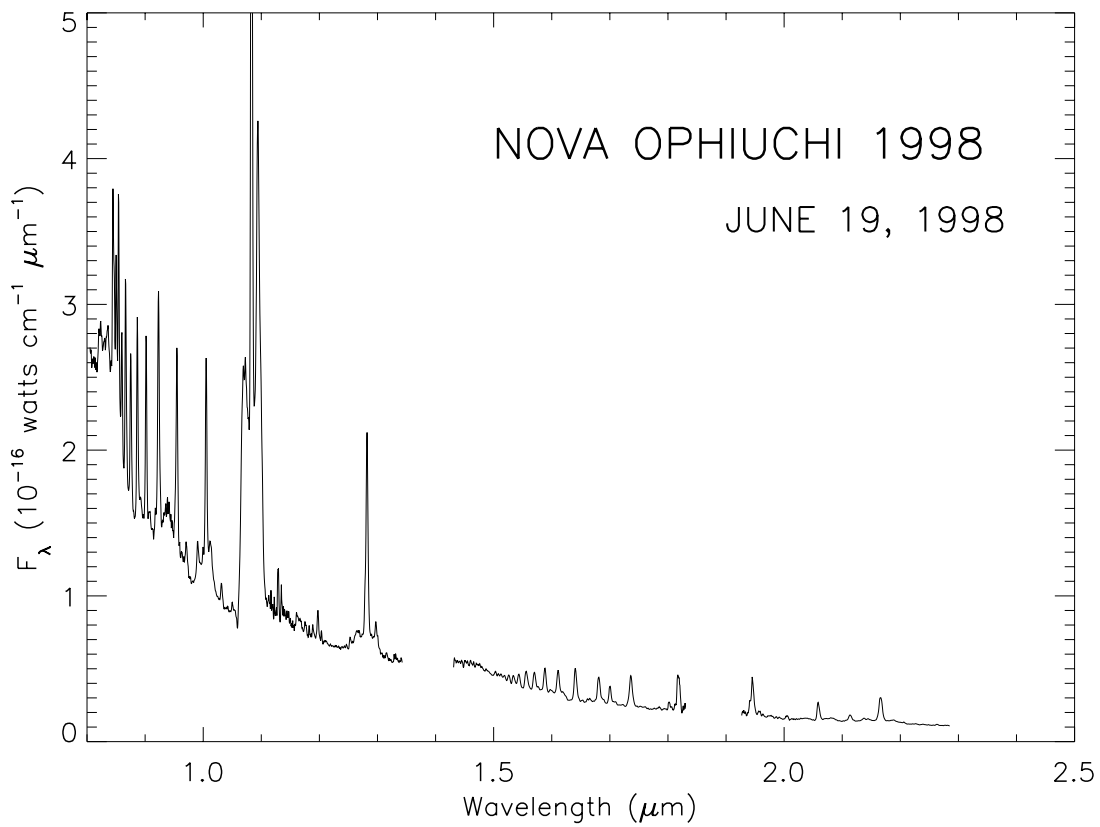


FIG. 3.—Spectrum from 1998 June 19.40, UT (JD 2,450,983.9)

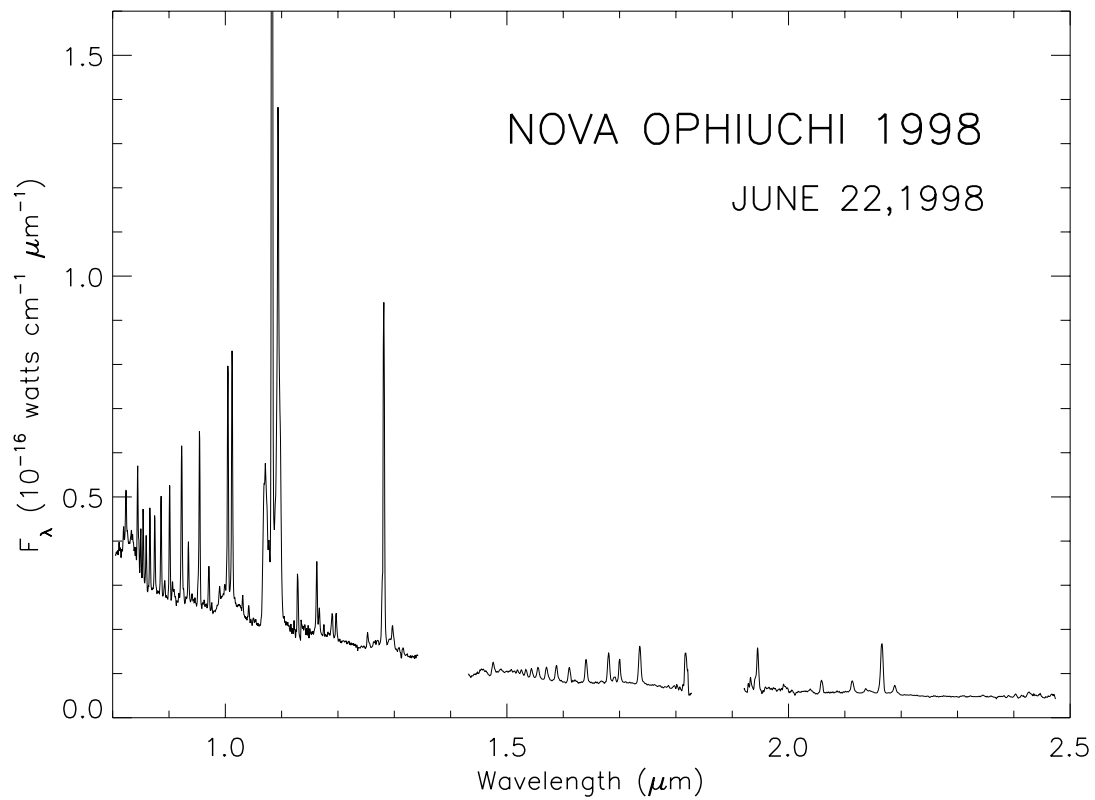


FIG. 4.—Spectrum from 1998 June 22.37, UT (JD 2,450,986.87)

TABLE 1
STANDARD STARS

Date (UT) (1998)	Star	Spectral Type	K Magnitude
Jun 19.40.....	HR 6715	K3 III	3.36
Jun 22.37.....	HD 161903	F0 V	7.02
Oct 2.17.....	HR 6743	F5 V	3.82

16'' error circle of the *ROSAT* source 1RXS 173200.0–191349.²

Nova Ophiuchi 1998 was an exceedingly fast nova as the optical light curve in Figure 1 shows (Mattei 1998, private communication). For the first couple of weeks after discovery the brightness decreased by about 0.32 mag day⁻¹, corresponding to t_2 and t_3 of 6.3 and 9.5 days, respectively. Thus the nova's speed class would be "very fast" according to Payne-Gaposchkin's guidelines (Payne-Gaposchkin 1957). After 18 days, the decline rate lessened to about 0.05 mag day⁻¹ until about day +45 when the decline appeared to stop and the magnitude remained constant near +15. As of our most recent measurements (1998 October) there was no indication of dust formation, although dust could have formed and then dissipated between our observations dates. Although the nova seems to have been discovered during the early stages of decline, its precise date of peak brightness is not known. Based on observations reported in the IAU Circulars, we have adopted the peak brightness and its date to be $m_p = 9.5$ and 1998 June 15.0 UT (JD 2,450,979.5), respectively.

In this paper we present near-IR spectroscopic observations of Nova Ophiuchi 1998 on the nights of 1998 June 19.40, June 22.37, and October 2.15 UT, roughly 4, 7, and 110 days after maximum. We analyze the spectral evolution and compare the results to previous novae measured at these wavelengths.

2. OBSERVATIONS

All observations were made with the Aerospace Corporation's Near Infrared Imaging Spectrograph (NIRIS) on the University of California's Lick Observatory 3 m Shane telescope. The spectrograph incorporates two separate channels, divided at 1.38 μm , to provide nearly continuous coverage between 0.8 and 2.5 μm . Each channel has its own collimator, grating, camera, and HgCdTe detector array. The arrays are 2 quadrant NICMOS3 devices providing 256 channels in the spectral dimension and 128 in the spatial at a scale of 1'' pixel⁻¹. Each channel has nearly constant spectral resolution. When using a 2'' slit width, the resolution is 14 Å for the blue channel, and 35 Å for the red. To facilitate background removal, spectra were acquired at 2 locations (separated by 10'') along the slit. Wavelength calibration was done by taking spectra of emission-line lamps.

The data were reduced in the normal manner using nearby comparison stars to remove the instrumental response and most of the effects of atmospheric absorption, and to estimate the absolute flux level for the nova. Because of the absence of a well-established infrared standard near

in the sky to the nova, we used three separate comparison stars (Table 1). Flux calibration was performed by taking the spectral shapes of Kurucz (1991) and setting the level based on standard stars (Elias 1982).

3. SPECTRA

Figure 2 shows the three spectra of Nova Ophiuchi 1998 taken on 1998 June 19.40, June 22.37, and October 2.15, all UT (JD 2,450,983.9, 2,450,986.87, and 2,451,088.65, respectively), and Figures 3 and 4 show the individual spectra from the first two nights. Table 2 lists the lines present in the spectra along with their flux densities. Apart

TABLE 2
NOVA OPHIUCHI 1998 LINE LIST

WAVELENGTH (μm)	IDENTITY	FRACTION OF Pa β	
		98 Jun 19	98 Jun 22
0.8237.....	H II	...	0.118
0.8446.....	O I	0.388	0.155
0.8467.....	H I Pa17	0.172	...
0.8545.....	H I Pa15	0.419	0.106
0.8598.....	H I Pa14	0.254	0.063
0.8665.....	H I Pa13	0.629	0.156
0.875.....	H I Pa12	0.506	0.152
0.8863.....	H I Pa11	0.673	0.191
0.9015.....	H I Pa10	0.618	0.225
0.9229.....	H I Pa9	1.036	0.372
0.9345.....	He II	...	0.115
0.9545.....	He I Pa10	0.849	0.380
0.971.....	C III	0.118	0.096
0.9903.....	C II	0.138	0.036
1.0049.....	H I Pa δ	0.832	0.444
1.0126.....	He II	...	0.571
1.0316.....	...	0.072	0.033
1.0422.....	0.030
1.0831.....	He I	3.928	3.511
1.1287.....	O I	0.135	0.128
1.1636.....	He II	...	0.165
1.1675.....	He II	...	0.040
1.1901.....	0.047
1.1969.....	He I	0.097	0.065
1.2534.....	He I	...	0.034
1.2785.....	He I	0.168	0.097
1.2818.....	H I Pa β	1.000	1.000
1.4763.....	He II	...	0.040
1.5261.....	H I Br19	0.033	0.005
1.5342.....	H I Br18	0.032	0.010
1.5439.....	H I Br17	0.060	0.018
1.5557.....	H I Br16	0.117	0.026
1.5701.....	H I Br15	0.102	0.032
1.5881.....	H I Br14	0.126	0.035
1.6109.....	H I Br13	0.143	0.033
1.6407.....	H I Br12	0.219	0.048
1.6807.....	H I Br11	0.176	0.050
1.6983.....	0.002
1.7002.....	He I	0.093	0.038
1.7362.....	H I Br10	0.246	0.093
1.8174.....	H I Br9	0.271	0.137
1.9446.....	H I Br8	0.257	0.087
2.0581.....	He I	0.102	0.027
2.1132.....	He I	0.044	0.034
2.1655.....	H I Br γ	0.216	0.137
2.1882.....	He II	...	0.024

NOTE.— $F(\text{Pa}\beta) \text{ W cm}^{-2} = 5.19 \text{ E-19}$ (for Jun 19), $= 2.27 \text{ E-19}$ (for Jun 22).

² Data available at <http://www.kusastro.kyoto-u.ac.jp/vsnet/Mail/vsnet-alert>.

from the very rapid decrease in brightness between the first two observations, there are a number of spectral aspects worthy of comment.

The spectra are dominated by permitted neutral hydrogen and helium lines of the Paschen and Brackett series. The strongest line in each of the spectra is the He I $\lambda 1.0830$ line followed closely by Pa β . The O I lines at 0.8446 and 1.1287 μm were also prominent, indicating significant fluorescent excitation by Ly β (Bowen 1947). Weak He II lines were also present on June 19. Neither the Paschen nor Brackett lines in the June 19 spectra conformed to the case B values (Storey & Hummer 1995). In the three days between the first and second spectra the He II lines strengthened dramatically, indicating a rapid evolution to higher excitation conditions in the shell. During the same period, the C III line at 0.9710 μm ($3d^3D-3p^3P^o$) appeared, a line seen at this strength only in objects like Wolf-Rayet stars or in planetary nebula with large carbon overabundances (Rudy et al. 1991a). This line almost certainly indicates an excess of carbon, a not unexpected finding in view of the thermonuclear chemistry of novae. To our knowledge, this is the first time that the line has been seen in a nova.

Inspection of the spectra revealed no evidence for a long wave emission upturn indicative of thermal emission from dust. It is possible that dust formed and then dissipated during the interval between our observations, although the optical light curve revealed no evidence of dust formation (Fig. 1). The broad emission features underlying the H I and He I lines noted earlier (Filippenko et al. 1998; Rudy et al. 1998) are discussed in the next section.

4. VELOCITY STRUCTURE

On both the June 19 and 22 the H I and He I lines were accompanied by broad, symmetric, roughly flat emission wings whose FWHM corresponded to about 10,000 km s^{-1} . Figure 5 shows an expanded view of the continuum emission feature surrounding He I $\lambda 1.0830$. The departure from a normal spectrum is obvious. Pa δ , Pa β , and Br γ also have similar emission structure surrounding them. All four lines show extended emission with roughly symmetric ± 3000 – 4000 km s^{-1} Doppler shifts, although the exact velocity components (if they are due to Doppler effects) do not coincide. The extreme limits of detection correspond to full width zero intensity (FWZI) of about 11,000 km s^{-1} , roughly corresponding to the 12,000 km s^{-1} base widths reported for H α by Filippenko et al. (1998) on June 18.

The emission plateau underlying the He I $\lambda 1.0830$ line could be interpreted as a velocity-broadened He I line, perhaps with self-absorption owing to the high optical depths in this line's metastable lower level. Self-absorption could produce an artificial decrease in brightness leading to the impression that there are three components, a central narrow one and two symmetrically placed red- and blue-shifted components. Thus, the obvious emission feature at 1.07 μm just blueward of the main line could be a Doppler-shifted component, and a similar redshifted component could underlie Pa γ as well. The latter possibility is suggested by the disproportionately large line strength for Pa γ compared to Pa β and Pa δ on either side because there is no known line at this wavelength that has ever been seen in a

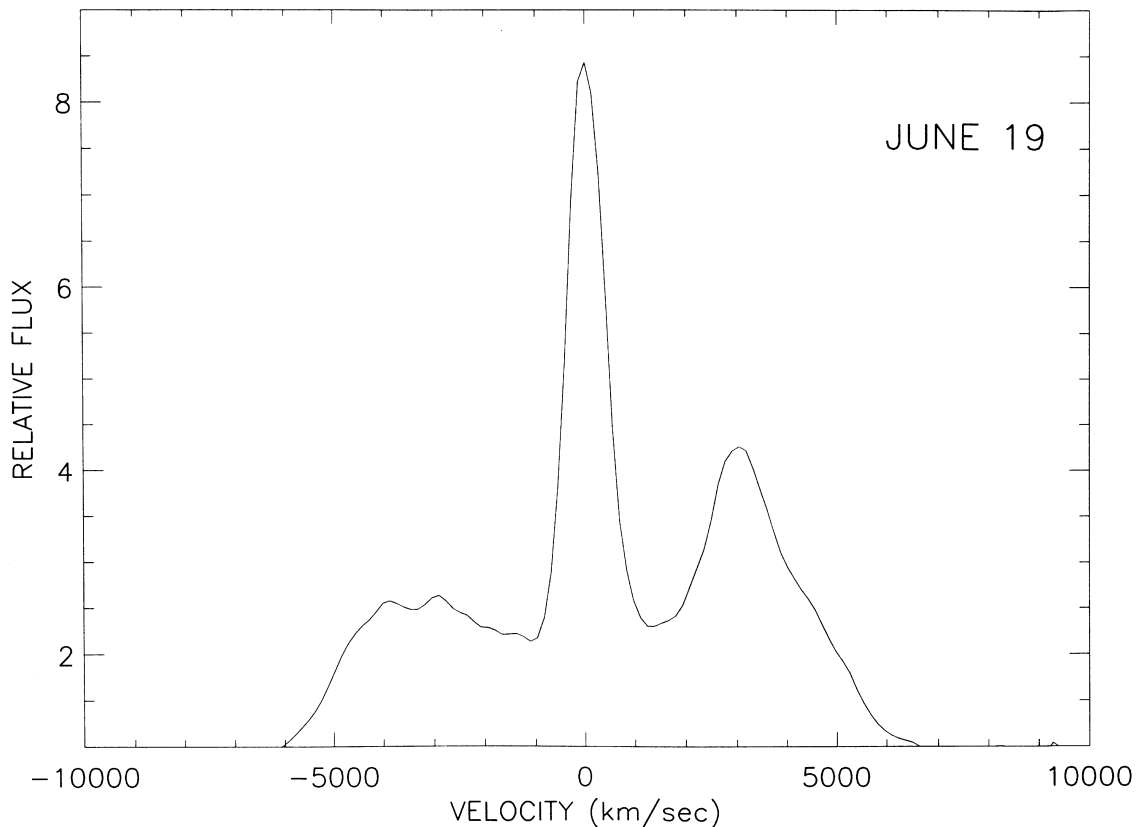


FIG. 5.—Spectral region around He I $\lambda 10830$. The abscissa is the velocity measured from the center of the narrow component of $\lambda 10830$. The structure under the narrow line is the broad component of $\lambda 10830$ augmented on the red wing by Pa γ . Note that wings of the line extend more than 5000 km s^{-1} from the line center.

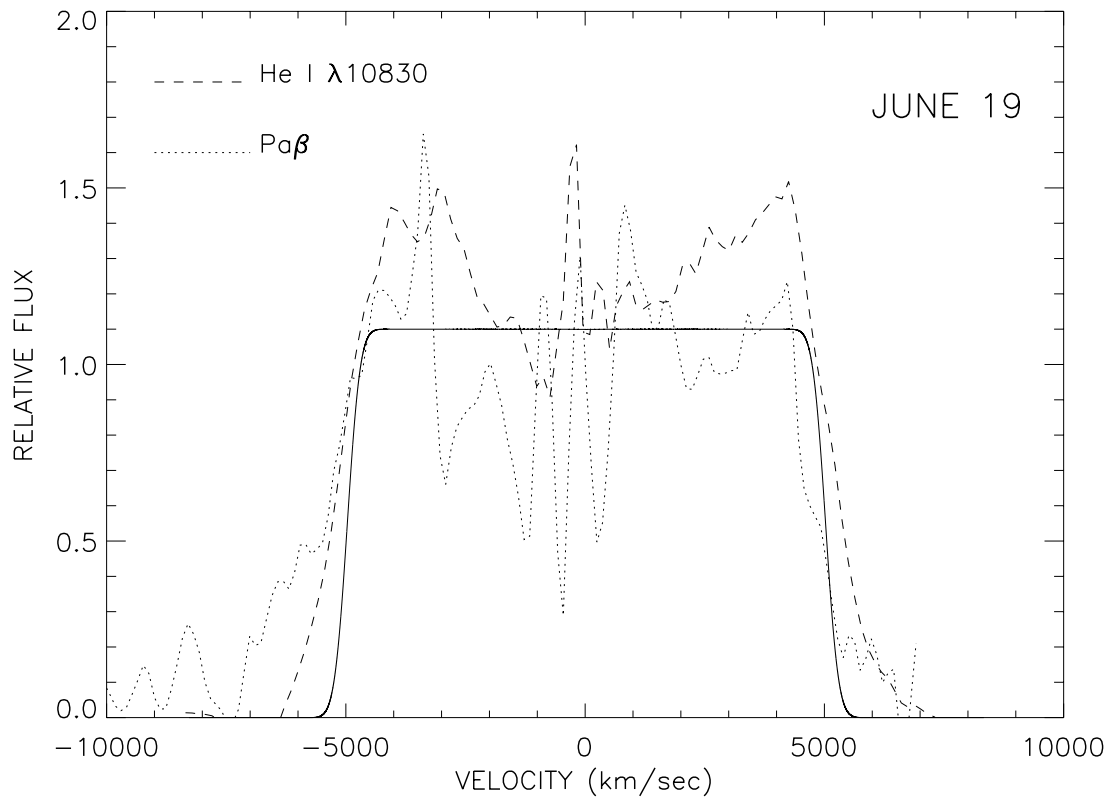


FIG. 6.—Same as Fig. 5, but with the narrow component of He I $\lambda 10830$ and the continuum removed. The broad component of Pa β , scaled to match $\lambda 10830$, is also shown. The large-amplitude variations in the observed profiles are artifacts introduced by removing the narrow components and are not significant. Note the large velocity widths and the similarities between the maximum H I and He I velocities. Also shown (solid line) is the theoretical line profile from an optically thin, spherical shell of gas expanding outward at 5000 km s^{-1} .

nova before. In classical novae, expansion velocities correlate with speed class, and the following empirical relations have been established (McLaughlin 1960):

$$\log V_{\text{exp}} = 3.70 - 0.5 \log t_3, \quad (1)$$

$$\log V_{\text{exp}} = 3.57 - 0.5 \log t_2, \quad (2)$$

where V_{exp} is in km s^{-1} and t_2 and t_3 is in days. Substituting $t_2 = 6.3$ days and $t_3 = 9.5$ days (from Fig. 1) we find $V_{\text{exp}} = 1470$ and 1630 km s^{-1} respectively, far below the observed velocities of $4000\text{--}5000 \text{ km s}^{-1}$ that was observed. On the other hand, expansion velocity—speed class correlations are statistical in nature and have significant scatter. For example, V838 Her 1991 and QU Vul both had expansion velocities exceeding 5000 km s^{-1} yet had very different decline rates (Harrison & Stringfellow 1994; Rosino et al. 1992). Thus the difference between the predicted and observed expansion velocities of Nova Oph 1998 are notable but probably not extreme.

5. REDDENING, INTRINSIC LUMINOSITY, AND DISTANCE

To estimate the nova's distance, we use the absolute magnitude and the extinction. Owing to the speed with which the nova evolved and the relatively normal looking spectra (except for the broad plateaus underlying the H I and He I lines), we believe that the nova was discovered very near its peak visual brightness, and therefore the observed value $m_v = 9.5$ does not seem unreasonable. The empirical relation between M_v and t_2 , the time it takes the nova's visual brightness to decrease by 2 mag (Cohen 1985; Capaccioli et

al. 1989; Schmidt 1967; Van den Bergh & Younger 1987, and extended by Della Valle & Livio 1995) suggests that

$$M_v(\text{peak}) = -7.92 - 0.81 \tan^{-1} [(1.32 - \log t_2)/0.23], \quad (3)$$

or $M_v = -8.8$ for $t_2 = 6.3$ days. The color excess $E(B-V)$ obtained from the O I $\lambda 8446$ and $\lambda 11287$ lines (Rudy et al. 1991a, b) was 0.38 ± 0.08 .

Extinction estimates based on COBE measurements (Schlegel, Finkbeiner, & Davis 1998) indicate that the maximum possible reddening in the direction is of Nova Oph 1998 is 0.62. This is consistent with our observations in the sense that the observed reddening (0.38) should be less than the COBE result (0.62), which it is. Contrary to earlier speculation that the novae could be suffering significant extinction owing to its location near the edge of dark cloud LDN195 (Kato 1998), the amount of reddening appears to be modest. Using our measured value obtained from the O I lines we find $A_v = 1.16 \pm 0.24$ magnitudes for an assumed reddening ratio $A_v/E(B-V) = 3.05$. The resulting distance is then 27.5 ± 3 kpc, placing the nova on the far side of the galaxy.

One mystery remains about this novae. Our spectrum from 1998 October 2 indicates that the magnitude at J was 15.0 at that time. The spectrum itself shows a starlike continuum with very weak emission lines. If the ejected shell had dissipated to the point where it was not emitting significantly, then the observed continuum emission would come from the combined continua of the two binary components.

Under such conditions, most of the infrared radiation should originate from the white dwarf's companion, which is a late-type dwarf in classical novae. Yet a main sequence K0 star, for example would have an apparent J magnitude of 22.9 at the distance 27 kpc and with the extinction of $A_v = 0.38$ found above, it would be even fainter. This is much dimmer than what is observed. Since it is unlikely that the companion star is 1–2 orders of magnitude more luminous than a K0V star, it is possible that the bulk of the emission we observed in October is from a “hot spot” remaining from the residual accretion disk. If so, the emission should continue to fade as the system returns to quiescence, behavior that will be apparent from photometric monitoring.

6. LINE PROFILES

Figure 6 shows the June 19 residual profile of the plateau after removing the narrow central component of He I $\lambda 1.0830$. The profile is roughly rectangular. A similar profile is obtained for the June 22 spectrum. Assuming that this emission was coming from an expanding shell of optically thin material of unknown shape, we computed a series of models using different geometries. We were able to match the observed line profiles by using an optically thin, spherical shell of gas expanding uniformly at 5000 km s^{-1} (also in Fig. 6). Although we cannot distinguish between a smooth shell and one composed of many discrete components, the fact that we can see the redshifted, back side shows that in a broad sense, the shell is transparent.

7. PASCHEN AND BRACKETT LINE RATIOS

As Table 2 and Figures 7 and 8 show, the line ratios of the narrow components depart strongly from case B values. Corrections for reddening do not help explain the observed ratios because reddening changes the case B line ratios in the wrong direction, making the decrement steeper, rather than less shallow as is observed. One potential explanation of the relative strength of the higher members of the Paschen line series is emission from high-density and/or optically thick emission-line gas. Strong emission in the upper series lines is often produced in emission-line cloud models for quasar broad-line regions (Hubbard & Puetter 1985a, b). Increased strength in the upper lines occurs when the level populations become thermalized at high densities ($n_e \geq 10^{10} \text{ cm}^{-3}$) or at large optical depths as radiative decays become progressively less important, relative to electron collisions, in determining the level populations.

To explore the effects of high densities and optically thick lines on the observed line ratios, we present a simple, illustrative calculation. It is not meant to be an accurate model of the formation of lines in a realistic emission-line region. Rather it is intended to test the importance of various physical processes. We shall develop a simple model in which we argue that the level populations above $n = 2$ are in (or at least near) thermal ratios in the region of the gas dominating line emission and we shall use simple, approximate formulae for the physical processes modeled. Nonetheless, the model demonstrates that the Paschen and Brackett emission must arise from optically thick, high-

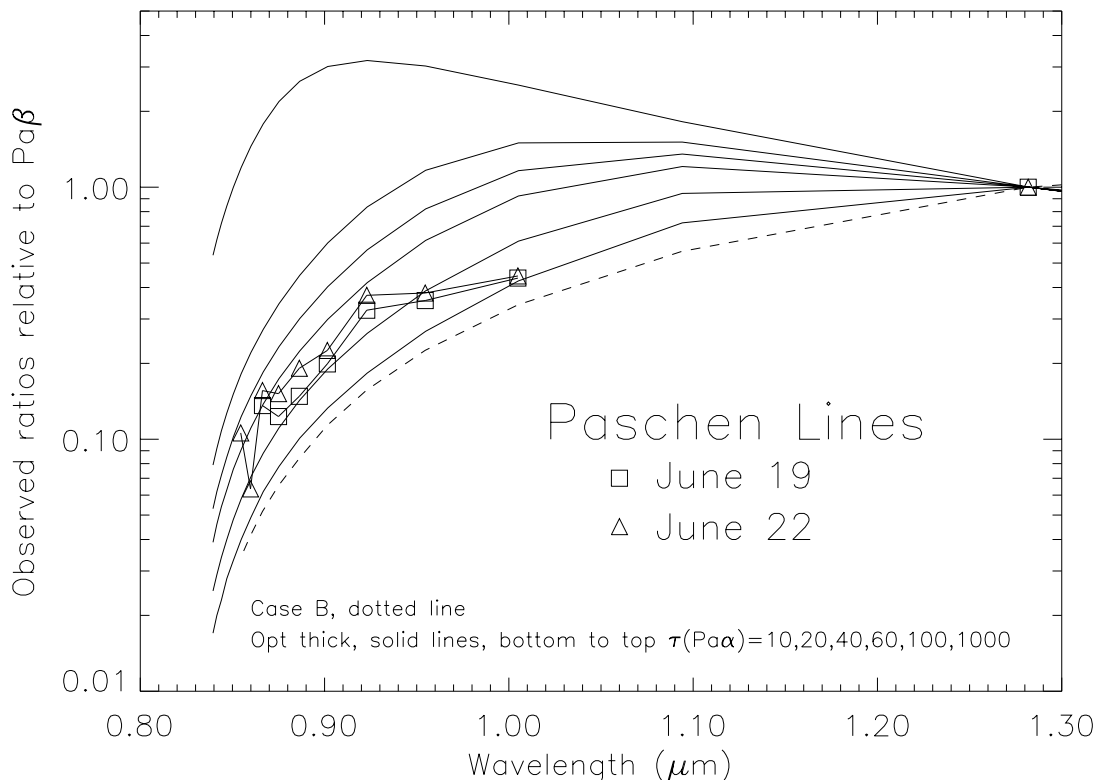


FIG. 7.—Theoretical Paschen line ratios (to $\text{Pa}\beta$) for various optical depths for $n_e = 6 \times 10^{10}$ and $T_e = 10,000 \text{ K}$. The case B values are shown as a dashed curve. The observed ratios (triangles and squares) follow the theoretical shapes and fall in the vicinity of $\tau(\text{Pa}\alpha) = 20\text{--}40$. Although the model may not embody all the physical properties of the nova shell, it does indicate that the observed departures from case B values can be explained in terms of large optical depths and high electron densities.

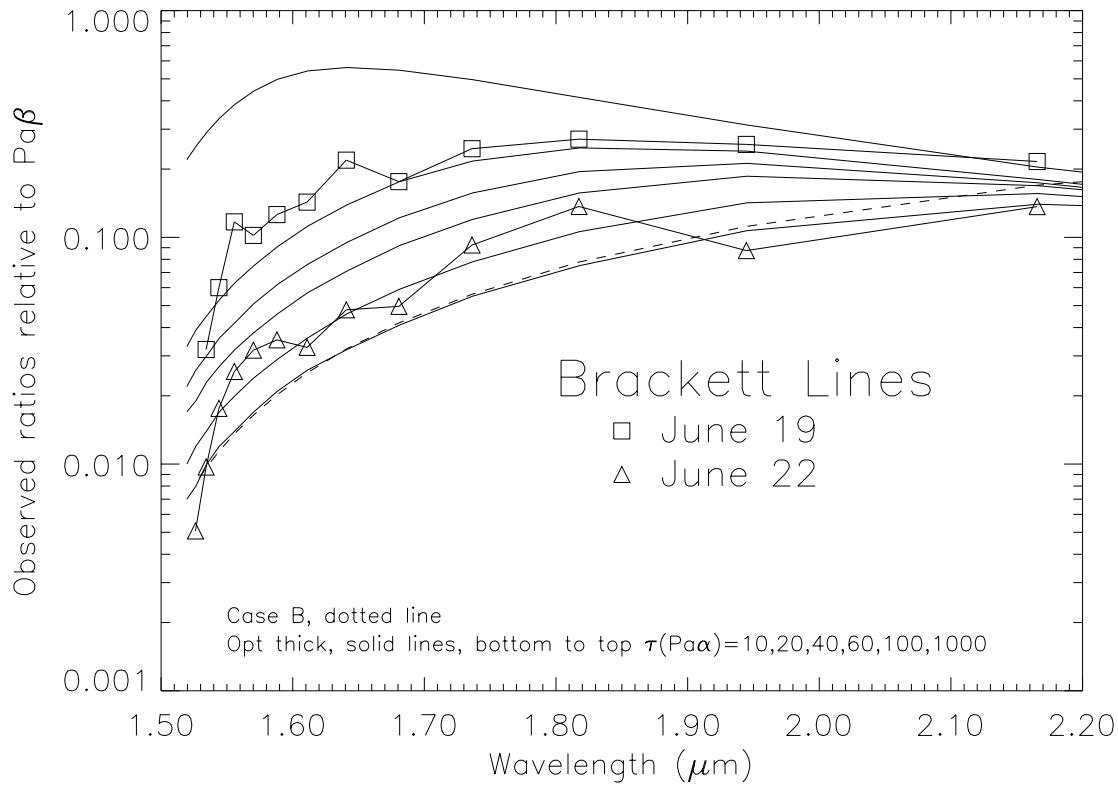


FIG. 8.—Same as Fig. 8, for the Brackett lines. Note the decrease in optical depth between June 19 and June 22 as the shell expands.

density gas in which both Doppler and Stark broadening are important. It further demonstrates that the lower lines of the series are optically thick and Doppler dominated, the middle lines being of modest thickness and Stark dominated, and the higher lines of the series being optically thin.

7.1. The Line Ratio Model

In order to explain the observed line ratios, we constructed a plane-parallel slab model of the shell with constant temperature and electron density. We then calculated the variation in line strengths as the uniform temperature, density, and total optical thickness of the slab were varied. We then computed the expected line fluxes and ratios using detailed balance. In order for the level populations above $n = 2$ to have populations in thermal ratios, the collisional deexcitation rates must dominate the net radiative downward rates. To perform a precise calculation, all collisional downward rates from a given level must be compared to all of the net downward radiative rates from that level. However, in the spirit of the approximate calculation presented here, we need only look at the “alpha” transition (i.e., the $n \rightarrow n - 1$ transition) to determine the approximate density at which collisional dominance sets in. In this case, we need for collisional dominance:

$$n_e q_{r \rightarrow s} \geq A_{r \rightarrow s} p_e(\tau_{r \rightarrow s}), \quad (4)$$

$$p_e(\tau) \equiv \frac{p_D^2(\tau)}{p_D(\tau) + p_S(\tau)} + \frac{p_S^2(\tau)}{p_D(\tau) + p_S(\tau)}, \quad (5)$$

$$p_D(\tau) = \frac{1}{2 + 4\sqrt{\pi\tau}\sqrt{\ln(1 + \tau)}}, \quad (6)$$

$$p_S(\tau) = \frac{1}{2 + 3.788\alpha_H(r, s)^{-2/5}\tau^{3/5}}, \quad (7)$$

$$\alpha_H(r, s) = 6.9 \times 10^{-6}(rs)^3\chi(r, s)\left(\frac{T_e}{10^4 \text{ K}}\right)\left(\frac{n_e}{10^{12} \text{ cm}^{-3}}\right), \quad (8)$$

$$\chi(r, s) = \begin{cases} 1/2, & \text{if } r = s + 1, \\ 1, & \text{if } r > s + 1, \end{cases} \quad (9)$$

$$\tau_{r \rightarrow s} = \frac{3h^3c^3}{8\pi E_{r \rightarrow s}^3} \sqrt{\frac{m_H}{2\pi k T_e}} A_{r \rightarrow s} L, \quad (10)$$

$$q_{r \rightarrow s} = \frac{8.629 \times 10^{-6} \text{ cm}^3 \text{ s}^{-1}}{r^2(T_e/\text{K})^{1/2}} \Omega_{r \rightarrow s}, \quad (11)$$

$$\Omega_{r \rightarrow s} = \frac{1.6\pi s^2 E_0}{\sqrt{3}} \frac{A_{r \rightarrow s}}{E_{r \rightarrow s} 3\gamma_{cl}(r \rightarrow s)}, \quad (12)$$

$$\gamma_{cl}(r \rightarrow s) = 2.5 \times 10^{-22} \left(\frac{E_{r \rightarrow s}}{h}\right)^2. \quad (13)$$

In equation (4), $q_{r \rightarrow s}$ is the collision coefficient for transitions from level r to level s , $A_{r \rightarrow s}$ is the spontaneous Einstein A coefficient, and p_e is the photon escape probability. Equation (5) gives a convenient approximation for the total photon escape probability when both Doppler and Stark redistribution of photons are important. This approximation has the correct behavior at zero optical depth and the correct asymptotic form when either Doppler redistrib-

TABLE 3
COLLISIONAL DOMINANCE DENSITIES

Transition	Optical Depth		
	$\tau(\text{Pa}\alpha) = 10$	$\tau(\text{Pa}\alpha) = 100$	$\tau(\text{Pa}\alpha) = 1000$
Pa α	3.0×10^{10}	2.2×10^9	1.7×10^8
Br α^a	3.8×10^8	3.0×10^7	2.6×10^6

^a Note that Br α optical depths assume thermal populations relative to $n = 3$.

bution or Stark redistribution dominate. This expression is easy to compute and is sufficiently accurate for the approximate calculations presented in this section. Equation (6)–(9) present the Doppler and Stark escape probabilities (Puetter 1981), where p_D is the Doppler escape probability and p_S is the Stark broadening escape probability. Equation (10) presents the formula for the line center optical depth, $\tau_{r \rightarrow s}$, where L is the path length through the media and E is the energy of the transition. Finally, equations (11)–(13) give the expression for the collision rates (see Lang 1978), where E_0 is the ionization energy of hydrogen. Again, these are approximate formulae, but their accuracy is sufficient for the purposes of the calculation presented here.

From the above equations, one can see that the $r \rightarrow s$ transition becomes collisionally dominated at an electron density of $n_{\text{crit}} \approx A_{r \rightarrow s} p_D(\tau_{r \rightarrow s}) / q_{r \rightarrow s}$. Some values of n_{crit} are given in Table 3 for the first transition of the Paschen and Brackett series.

If the above conditions apply, the upper level populations are dominated by collisions and are in ratios given by the thermal values. (This occurs rapidly at high densities even if the lower level populations are nonthermal.) If we make the approximation that the line emission is dominated from a region of the gas where the level populations are constant, a simple relationship for the observed line ratios for the Paschen and Brackett lines arises, and the relative line

strengths are given by

$$\frac{l_{n \rightarrow m}}{l_{r \rightarrow s}} = \frac{h\nu_{n \rightarrow m} n_n A_{n \rightarrow m} \int dL p_e(\tau_{n \rightarrow m})}{h\nu_{r \rightarrow s} n_r A_{r \rightarrow s} \int dL p_e(\tau_{r \rightarrow m})}. \quad (14)$$

In addition, if the level populations are thermalized the following relationship holds:

$$\frac{n_n}{n_r} = \frac{g_n}{g_r} \exp\left(\frac{-\Delta E_{n \rightarrow r}}{kT_e}\right), \quad (15)$$

where g_n is the statistical weight of level n . Results for the Paschen and Brackett series line for several temperatures, densities, and optical depths are given in Table 4. The electron densities in Table 4 were selected to guarantee collisionally dominated level populations, with the lowest density represented equaling roughly twice that needed for collisional dominance of Pa α (see Table 5). The limiting case of optical thin emission is not dependent on density (so long as the level populations are thermal) and is given in Tables 5 and 6 for $n_e = 6 \times 10^{10} \text{ cm}^{-3}$ and $6 \times 10^{11} \text{ cm}^{-3}$, respectively. For reference, these line ratios can be compared to the observed line ratios on June 19, given in Table 2.

Comparison of the theoretical line ratios in Tables 4 and 5 with the observed line ratios in Table 2 immediately provide the following conclusions: (1) Optically thin emission, even if the level populations are thermalized, this does not sufficiently increase the higher series members sufficiently to explain the data. (2) Optically thick emission is required to cause the Paschen line ratios to peak near Pa8 or Pa9. Optically thick emission is also required to increase the emission in the higher Brackett lines relative to Pa β . (3) The details of the optically thick emission are clearly more complicated than described in the simple model described here. Nonetheless, optical depths in Pa α less than 1000 are suggested in order to cause the Brackett line ratios to drop rapidly past Pa15–Pa18.

Another interesting aspect of the optically thick models presented here is the strong depression of emission in Pa α and Br α . Depressed emission in Pa α has been noted previously in emission-line studies of broad-line emission in QSO and AGNs (e.g., in NGC1275; see Lacy et al. 1982).

Figures 7 and 8 show the theoretical models for the Paschen and Brackett lines, respectively. For these calculations we used $n_e = 6 \times 10^{10}$ and $T_e = 10,000 \text{ K}$. The case B values are shown as a dashed curve. Optical depths in the Pa α line of 10, 20, 40, 60, 100, and 1000 are shown. The observed ratios follow the trends present in the theoretical models and indicate optical depths between 20 and 40 in Pa α for the Paschen series and between 10 and a few hundred in Pa α for the Brackett series. The discrepancy between the two series is probably due to the lines forming in slightly different regions of the emission-line gas (i.e., due to nonconstant source function effects as was assumed here). Given the simplicity of the model, we feel they produce remarkably good results. In addition, the drop in the optical depth between June 19 and 22 is undoubtedly real and probably results from the gas expanding and becoming less dense and optically thick in these transitions.

From the above equations and the sample values of the line ratios, one can see that thermalized emission can qualitatively explain the lack of a case B decrement in the

TABLE 4
PASCHEN AND BRACKETT LINE RATIOS: THERMALIZED POPULATIONS, OPTICALLY THIN EMISSION

Line	$T_e = 5 \times 10^3 \text{ K}$	$T_e = 1 \times 10^4 \text{ K}$	$T_e = 1.5 \times 10^4 \text{ K}$
Pa α	1.829	1.789	1.786
Pa β	1.000	1.000	1.000
Pa γ	0.588	0.596	0.597
Pa δ	0.373	0.380	0.381
Pa8	0.250	0.257	0.258
Pa9	0.176	0.181	0.182
Pa10	0.128	0.133	0.133
Pa12	0.074	0.077	0.077
Pa15	0.038	0.040	0.040
Pa18	0.022	0.023	0.023
Pa20	0.016	0.017	0.017
Br α	0.385	0.387	0.387
Br β	0.242	0.246	0.246
Br γ	0.256	0.160	0.160
Br δ	0.106	0.109	0.109
Br9	0.075	0.077	0.077
Br10	0.055	0.057	0.057
Br12	0.032	0.033	0.033
Br15	0.016	0.017	0.017
Br18	0.009	0.010	0.010
Br20	0.007	0.007	0.007

TABLE 5
 PASCHEN AND BRACKETT LINE RATIOS^a: THERMALIZED POPULATIONS, $n_e = 6 \times 10^{10} \text{ cm}^{-3}$

LINE	$T_e = 5 \times 10^3 \text{ K}$			$T_e = 1 \times 10^4 \text{ K}$			$T_e = 1.5 \times 10^4 \text{ K}$		
	$\tau = 10$	$\tau = 10^2$	$\tau = 10^3$	$\tau = 10$	$\tau = 10^2$	$\tau = 10^3$	$\tau = 10$	$\tau = 10^2$	$\tau = 10^3$
Pa α	0.614	0.394	0.398	0.432	0.281	0.300	0.381	0.255	0.284
Pa β	1.000	1.000	1.000	1.000	1.000	1.000	1.000	1.000	1.000
Pa γ	0.596	1.245	1.528	0.722	1.510	1.819	0.771	1.609	1.928
Pa δ	0.310	1.101	1.927	0.425	1.499	2.542	0.473	1.662	2.789
Pa8	0.179	0.794	2.111	0.268	1.167	3.026	0.308	1.329	3.402
Pa9	0.115	0.537	2.107	0.183	0.835	3.182	0.216	0.971	3.641
Pa10	0.080	0.369	1.920	0.133	0.601	3.013	0.159	0.711	3.494
Pa11	0.059	0.265	1.628	0.101	0.447	2.632	0.121	0.537	3.086
Pa12	0.045	0.198	1.321	0.078	0.345	2.189	0.095	0.418	2.591
Pa13	0.035	0.154	1.054	0.062	0.273	1.784	0.075	0.334	2.131
Pa14	0.028	0.123	0.843	0.049	0.221	1.455	0.060	0.271	1.752
Pa15	0.222	0.100	0.683	0.040	0.182	1.198	0.049	0.224	1.452
Pa16	0.018	0.082	0.561	0.033	0.151	0.998	0.041	0.187	1.217
Pa17	0.015	0.069	0.468	0.028	0.127	0.842	0.034	0.157	1.032
Pa18	0.013	0.058	0.396	0.023	0.108	0.719	0.029	0.133	0.883
Pa19	0.011	0.050	0.339	0.020	0.092	0.619	0.024	0.114	0.761
Pa20	0.009	0.043	0.293	0.017	0.079	0.537	0.021	0.098	0.662
Br α	0.055	0.038	0.047	0.030	0.023	0.033	0.024	0.021	0.032
Br β	0.151	0.143	0.150	0.116	0.092	0.103	0.103	0.081	0.096
Br γ	0.121	0.231	0.279	0.140	0.180	0.204	0.143	0.164	0.192
Br δ	0.075	0.245	0.398	0.107	0.240	0.313	0.119	0.232	0.296
Br9	0.048	0.202	0.485	0.075	0.248	0.414	0.087	0.257	0.396
Br10	0.034	0.150	0.526	0.055	0.217	0.496	0.064	0.240	0.483
Br11	0.025	0.111	0.517	0.041	0.176	0.546	0.049	0.202	0.546
Br12	0.019	0.084	0.476	0.032	0.139	0.561	0.039	0.165	0.578
Br13	0.015	0.065	0.405	0.026	0.112	0.542	0.031	0.134	0.578
Br14	0.012	0.052	0.339	0.021	0.091	0.498	0.025	0.110	0.550
Br15	0.010	0.043	0.282	0.017	0.705	0.442	0.021	0.091	0.503
Br16	0.008	0.035	0.235	0.014	0.063	0.386	0.017	0.077	0.449
Br17	0.006	0.030	0.198	0.012	0.053	0.335	0.014	0.065	0.396
Br18	0.005	0.025	0.169	0.010	0.045	0.290	0.012	0.055	0.347
Br19	0.005	0.021	0.145	0.008	0.039	0.252	0.010	0.048	0.304
Br20	0.004	0.018	0.125	0.007	0.033	0.220	0.009	0.041	0.267

^a The optical depths given are line center optical depths in Paschen alpha.

Paschen and Brackett series. A more realistic model must include the variation of the line source functions as one moves into the emission-line gas. Such a model is beyond the scope of this paper. However, the above calculation demonstrates the importance of level thermalization and optical depth effects in producing the observed emission.

In summary, we believe that the conditions in the nova shell can be broadly characterized as having temperatures near 10,000 K, optical depths in the cores of Pa α of between 10 and 100, and electron density of order 10^{11} cm^{-3} . This is based on a simple plane-parallel slab model of the shell. These values are necessary in order to explain the observed deviations of the Paschen and Brackett lines from case B values.

8. SUMMARY AND CONCLUSIONS

Nova Ophiuchi 1998 displayed several unusual features:

(1) It was one of the fastest nova ever observed; (2) the C III line $3d \ ^3D-3p \ ^3P^o$ at $0.9710 \ \mu\text{m}$ indicates a probable overabundance of carbon; (3) it displayed velocity structure in the H I and He I lines in the form of bright narrow components and faint broad components; (4) the H I and He I lines showed strong departures from case B values indicative of very dense regions ($n_e = 10^{11} \text{ cm}^{-3}$) or large optical depths ($10-10^2$), or both.

We would like to thank Carl J. Rice and Theo. K. Tessensohn for logistical support. We would also like to thank Wayne Earthman, Keith Baker, and Kostas Chloros for expert telescope operation.

TABLE 6
 PASCHEN AND BRACKETT LINE RATIOS^a: THERMALIZED POPULATIONS, $n_e = 6 \times 10^{11} \text{ cm}^{-3}$

LINE	$T_e = 5 \times 10^3 \text{ K}$			$T_e = 1.5 \times 10^4 \text{ K}$			$T_e = 1 \times 10^4 \text{ K}$		
	$\tau = 10$	$\tau = 10^2$	$\tau = 10^3$	$\tau = 10$	$\tau = 10^2$	$\tau = 10^3$	$\tau = 10$	$\tau = 10^2$	$\tau = 10^3$
Pa α	0.617	0.453	0.554	0.440	0.348	0.437	0.398	0.330	0.414
Pa β	1.000	1.000	1.000	1.000	1.000	1.000	1.000	1.000	1.000
Pa γ	0.600	1.236	1.415	0.735	1.485	1.645	0.789	1.570	1.706
Pa δ	0.323	1.099	1.715	0.451	1.487	2.193	0.509	1.636	2.327
Pa8	0.195	0.801	1.878	0.297	1.179	2.564	0.344	1.338	2.767
Pa9	0.129	0.555	1.875	0.207	0.869	2.690	0.245	1.009	2.944
Pa10	0.091	0.394	1.721	0.151	0.645	2.566	0.180	0.761	2.844
Pa11	0.066	0.290	1.476	0.113	0.491	2.272	0.136	0.586	2.546
Pa12	0.050	0.222	1.217	0.087	0.383	1.925	0.105	0.459	2.177
Pa13	0.038	0.173	0.991	0.068	0.304	1.601	0.082	0.366	1.824
Pa14	0.030	0.138	0.809	0.054	0.245	1.328	0.066	0.296	1.522
Pa15	0.024	0.112	0.667	0.044	0.200	1.108	0.053	0.243	1.275
Pa16	0.020	0.092	0.555	0.036	0.166	0.931	0.044	0.201	1.074
Pa17	0.016	0.077	0.467	0.030	0.138	0.788	0.036	0.168	0.910
Pa18	0.014	0.064	0.397	0.025	0.117	0.672	0.031	0.142	0.777
Pa19	0.012	0.054	0.339	0.021	0.099	0.577	0.026	0.121	0.668
Pa20	0.010	0.047	0.293	0.018	0.085	0.499	0.022	0.104	0.577
Br α	0.060	0.055	0.085	0.038	0.041	0.064	0.035	0.040	0.061
Br β	0.151	0.150	0.182	0.118	0.110	0.148	0.108	0.105	0.144
Br γ	0.124	0.233	0.293	0.144	0.192	0.250	0.148	0.185	0.247
Br δ	0.080	0.248	0.388	0.114	0.248	0.342	0.127	0.245	0.339
Br9	0.054	0.208	0.456	0.083	0.257	0.419	0.096	0.268	0.415
Br10	0.038	0.159	0.488	0.062	0.229	0.476	0.073	0.252	0.473
Br11	0.028	0.121	0.480	0.047	0.189	0.509	0.056	0.217	0.509
Br12	0.021	0.093	0.440	0.036	0.153	0.515	0.044	0.179	0.523
Br13	0.016	0.074	0.385	0.029	0.124	0.495	0.035	0.147	0.515
Br14	0.013	0.059	0.328	0.023	0.101	0.457	0.028	0.121	0.487
Br15	0.010	0.048	0.277	0.019	0.084	0.409	0.023	0.100	0.445
Br16	0.008	0.039	0.234	0.015	0.069	0.360	0.019	0.084	0.398
Br17	0.007	0.033	0.198	0.013	0.058	0.313	0.016	0.070	0.352
Br18	0.006	0.028	0.169	0.011	0.049	0.273	0.013	0.060	0.308
Br19	0.005	0.023	0.145	0.009	0.042	0.237	0.011	0.051	0.270
Br20	0.004	0.020	0.125	0.008	0.036	0.207	0.010	0.044	0.236

^a The optical depths given are line center optical depths in Paschen alpha.

REFERENCES

- Bowen, I. S. 1947, *PASP*, 59, 196
 Capaccioli, M., Della Valle, M., D'Onofrio, M., & Rosino, L. 1989, *AJ*, 97, 1622
 Cohen, J. G. 1985, *ApJ*, 292, 90
 Della Valle, M., & Livio, M. 1995, *ApJ*, 452, 704
 Elias, J., Frogel, J. A., Matthews, K., & Neugebauer, G. 1982, *AJ*, 87, 1029
 Erwin, P., Lynch, D. K., Rudy, R. J., Rossano, G. S., & Puetter, R. C. 1992, *AJ*, 103, 1970
 Filippenko, A., Leonard, D. C., & Modjaz, M. 1998, *IAU Circ.* 6943
 Gallagher, J., Hege, E. K., Kopriva, D. A., Williams, R. E., & Butcher, H. R. 1980, *ApJ*, 237, 22
 Hanzl, D. 1998, *IAU Circ.* 6943
 Harrison, T. E., & Stringfellow, G. E. 1994, *ApJ*, 437, 827
 Hubbard, E. N., & Puetter, R. C. 1985a, *ApJ*, 290, 394
 ———, 1985b, *ApJ*, 295, 394
 Kurucz, R. L. 1991, *Precision Astronomy: Astrophysics of the Galaxy*, ed. A. G. Davis Philip, A. R. Upgren, & K. A. Janes (Schenectady, NY: Davis), 27
 Lacy, J. H., Malkan, M., Becklin, E. E., Soifer, B. T., Neugebauer, G., Matthews, K., Wu, C.-C., Boggess, A., & Gull, T. R. 1982, *ApJ*, 256, 75
 Lang, K. R. 1978, *Astrophysical Formulae*, (Berlin: Springer)
 Lynch, D. K., Rossano, G. S., Rudy, R. J., & Puetter, R. C. 1995, *AJ*, 98, 2274
 Lynch, D. K., Rudy, R. J., Rossano, G. S., Erwin, P. H., & Puetter, R. C. 1989, *AJ*, 98, 1682
 MacDonald, J. 1984, *ApJ*, 273, 289
 McLaughlin, D. B. 1960, in *Stellar Atmospheres*, ed. J. L. Greenstein (Chicago: Univ. Chicago Press)
 Nakano, S., Takamizawa, K., Kushida, T., & Kato, T. 1998, *IAU Circ.* 6941
 Payne-Gaposchkin, C. 1957, *The Galactic Novae*, (Amsterdam: North Holland)
 Prialnik, D., & Kovetz, A. 1984, *ApJ*, 281, 367
 Puetter, R. C. 1981, *ApJ*, 251, 446
 Rosino, L., Iijima, T., Benetti, S., D'Ambrosio, V., di Paolantonio, A., & Kolotilov, E. A. 1992, *A&A*, 257, 603
 Rudy, R. J., Cohen, R. D., Rossano, G. S., Erwin, P., Puetter, R. C., & Lynch, D. K. 1991b, *ApJ*, 380, 151
 Rudy, R. J., Erwin, P., Rossano, G. S., & Puetter, R. C. 1991a, *ApJ*, 383, 343
 Rudy, R. J., Tessensohn, T. K., Mazuk, S., Rice, C. J., Lynch, D. K., & Puetter, R. C. 1998, *IAU Circ.* 7049
 Schlegel, D., Finkbeiner, D., & Davis, M. 1998, *ApJ*, 500, 525
 Schmidt, T. 1967, *Z. Astrophys.*, 41, 182
 Starrfield, S. 1989, in *Classical Novae*, ed. M. F. Bode, & A. Evans (London: Wiley), chapter 3
 Storey, P. J., & Hummer, D. G. 1995, *MNRAS*, 292, 41
 Van den Bergh, S., & Younger, P. F. 1987, *A&A*, 70, 125
 Williams, R. E., & Gallagher, J. S. 1979, *ApJ*, 228, 482
 Williams, R. E., Woolf, N. J., Hege, E. K., Moore, R. L., & Kopriva, D. J. 1978, *ApJ*, 224, 171